CrystEngComm

Accepted Manuscript

ROYAL SOCIETY OF CHEMISTRY

www.rsc.org/crystengcomm

Journal Name

RSCPublishing

COMMUNICATION

Facile Synthesis of Ternary Homogeneous $ZnS_{1-x}Se_x$ Nanosheets with Tunable Bandgaps

Cite this: DOI: 10.1039/x0xx00000x

Jing Sun, Yumin Chen, Zhong-Ning Xu, Qing-Song Chen, Guan-E Wang, Ming-Jian Zhang, Gang Lu, Ke-Chen Wu* and Guo-Cong Guo*

Received 00th January 2012,
Accepted 00th January 2012

DOI: 10.1039/x0xx00000x

www.rsc.org/

The rational design and synthesis of ternary two-dimensional alloy nanocrystals with a non-layered structure still remains a challenge. Here, we show that, for the first time, the synthesis of homogeneous ternary $ZnS_{1-x}Se_x$ nanosheets by thermal decomposing of lamellar inorganic-organic hybrid precursors. The morphology, composition and crystal structure of $ZnS_{1-x}Se_x$ nanosheets have been thoroughly investigated. We also found that the lattice constants and bandgaps of $ZnS_{1-x}Se_x$ nanosheets could be easily tuned via altering Se/S ratio. Our work provides a facile and effective strategy to synthesize homogeneous multinary non-layered chalcogenide nanosheets with tunable compositions and bandgaps.

Two-dimensional (2D) semiconductor chalcogenide nanocrystals (NCs) have recently aroused wide interest due to their unique electronic band structure[1], and potential applications in various fields including optics, electronics, catalysis, and mechanics.[2-5] However, in order to make these 2D NCs more versatile, further modification of their band structure is required, which could correspondingly tune their properties. Fabrication of alloy NCs with tunable compositions is a possible way to fine-tune their band structures. However, only a few ternary chalcogenide alloy nanosheets with complete composition tunability have been reported to date. Very recently, composition-dependent $Mo_{1-x}W_xS_2$,[6] $MoS_{2x}Se_{2(1-x)}$,[7, 8] $Bi_2Se_{3-x}Te_x$,[9] $Sn_xGe_{1-x}Se$ [10] nanosheets have been achieved. However, these reported examples are still limited to layer chalcogenide compounds.[1, 11] In other words, for non-layered chalcogenide compounds (such as II-IV semiconductors with wurtzite and zinc blende crystal structure), the syntheses of ternary alloy nanosheets with tunable compositions are still greatly underdeveloped. First, traditional exfoliation method is not efficient for non-layered compounds to achieve 2D morphology considering the strong in-plane bonds.[12] Though recently there are a few reports on direct growth of binary 2D NCs with a non-layered structure,[13-17] the excess metal ion and organic ligands with a long hydrocarbon chain are generally required, which unfortunately bring a challenge to synthesize ternary 2D nanosheets with controlled composition. Second, since the cation or anion precursors often have different chemical reactivities, it is difficult to balance their relative reactivities to achieve desired composition and homogeneous internal structure of alloy NCs,[18-20] which could consequently influence the accuracy of bandgap that is of central importance for optoelectronic application with tunable spectral responses.[8]

A simple lamellar inorganic-organic hybrid intermediate strategy has been adopted in the syntheses of 2D NCs with a non-layered structure,[11, 21-26] but these cases are limited to binary chalcogenide NCs. In this communication, taking typical ternary non-layered zinc sulfur selenium ($ZnS_{1-x}Se_x$) as examples, we show, for the first time ternary alloy nanosheets with tunable compositions can be simply fabricated via the hybrid intermediate strategy. Besides, we have tried to overcome the differences in reactivity of S and Se precursors by using thioacetamide (TAA) and Se powder. Then, the complete composition tunability and homogeneity of the $ZnS_{1-x}Se_x$ nanosheets have been demonstrated. Furthermore, the effect of

State Key Laboratory of Structural Chemistry, Fujian Institute of Research on the Structure of Matter, Chinese Academy of Sciences, Fuzhou, Fujian 350002, P. R. China

† Electronic Supplementary Information (ESI) available: Experimental details and characterization data of $ZnS_{1-x}Se_x$ nanosheets and $ZnS_{1-x}Se_x$·0.5en precursors. See DOI: 10.1039/c000000x/

the compositions on the bandgaps and optical properties of ternary $ZnS_{1-x}Se_x$ nanosheets has also been investigated.

The ternary phase-pure $ZnS_{1-x}Se_x$ nanosheets were successfully synthesized by simply calcining the lamellar precursor $ZnS_{1-x}Se_x$·0.5en (en stands for ethylenediamine), in which $ZnS_{1-x}Se_x$·0.5en were initially fabricated via a hydrothermal process (Figure S1). The detailed syntheses and characterizations of $ZnS_{1-x}Se_x$ nanosheets and $ZnS_{1-x}Se_x$·0.5en precursors were shown in ESI†.

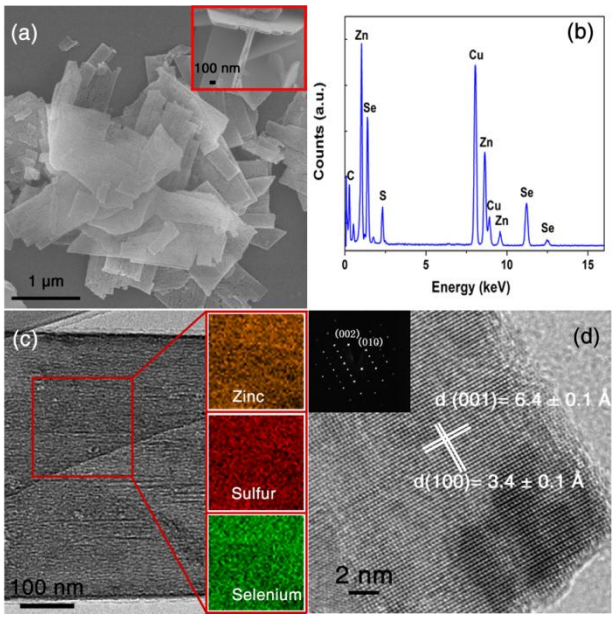

Figure 1 (a) SEM image of ternary $ZnS_{0.4}Se_{0.6}$ nanosheets. The inset SEM image suggests the thickness of the sheets is about 60nm. (b) EDX spectrum of ternary $ZnS_{0.4}Se_{0.6}$ nanosheets. (c) TEM and EDS mapping images of an individual ternary $ZnS_{0.4}Se_{0.6}$ nanosheet. (d) HRTEM image and SAED pattern (inset) of the $ZnS_{0.4}Se_{0.6}$ nanosheet.

A typical scanning electron microscopy (SEM) image in Figure 1a reveals that the morphology of the resulting nanocrystals is nanosheet with the edge lengths of 0.1-5 μm. The thickness is in range of 40-80 nm (see the typical SEM image in the inset of Figure 1a). Transmission electron microscopy (TEM) combined with energy-dispersive X-ray spectroscopy (EDX) was used to investigate the composition, homogeneity and microstructure. The EDX spectrum shown in Figure 1b demonstrates that the nanosheets exclusively consist of Zn, S, and Se elements. In addition, C and Cu elements come from the TEM copper grid. The EDX elemental mapping images of an individual nanosheet (Figure 1c) further confirm the chemical compositions, and intuitively reveal that Zn, S and Se are homogeneously distributed in a single nanosheet. The SAED pattern (inset of Figure 1d) indicates that the nanosheets are single-crystalline with hexagonal crystal structure. The corresponding high resolution TEM (HRTEM) image displays that its (001) and (100) interplanar spacings are about 0.64 nm and 0.34 nm respectively, consistent with previous reports. [27-30] The SEM, TEM and EDX elemental mapping images of other representative samples with various compositions are shown in Figure S2-4.

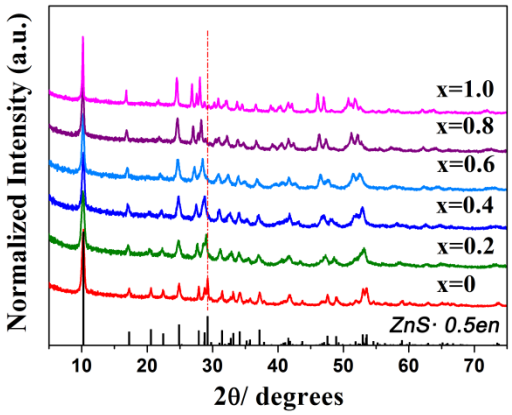

Figure 2 The XRD patterns of the $ZnS_{1-x}Se_x$·0.5en precursors for various values of x. The standard XRD patterns for ZnS·0.5en was shown below.

Before we prepared a series of $ZnS_{1-x}Se_x$ nanosheets with different Se/S ratios, the lamellar precursor ($ZnS_{1-x}Se_x$·0.5en) was firstly investigated by XRD (Figure 2) and SEM. Comparing the XRD patterns of $ZnS_{1-x}Se_x$·0.5en with that of ZnS·0.5en, we found that they have the same orthorhombic *Pbca* crystal structure.[21] It suggests that these precursors with various Se/S ratios all possess hexagonal $ZnS_{1-x}Se_x$ slab similar to ZnS·0.5en.[31] Besides, a gradual shift to lower 2θ degrees was observed as the Se content increased, which indicated the successful incorporation of Se atoms. The typical SEM and TEM images (Figure S5-S6) confirm the lamellar morphology of inorganic-organic hybrid precursors. These results reveal that Se atoms have been successfully alloyed into the lamellar precursor without changing their morphology, which is the most crucial for the successful fabrication of ternary $ZnS_{1-x}Se_x$ nanosheets in our case.

Table 1 The composition analysis of $ZnS_{1-x}Se_x$ nanosheets

Calculated Composition	Zn : S : Se ratio (determined by EDX)
ZnS (x=0)	1.02 : 0.98 : 0
$ZnS_{0.8}Se_{0.2}$ (x=0.2)	1.03 : 0.77 : 0.20
$ZnS_{0.6}Se_{0.4}$ (x=0.4)	1.05 : 0.57 : 0.38
$ZnS_{0.4}Se_{0.6}$ (x=0.6)	1.05 : 0.40 : 0.55
$ZnS_{0.2}Se_{0.8}$ (x=0.8)	1.02 : 0.19 : 0.79
ZnSe (x=1)	1.01 : 0.99 : 0

In order to demonstrate the complete composition tunability, we have prepared a series of $ZnS_{1-x}Se_x$ nanosheets with different x value. The composition of the alloy nanosheets was modulated by varying the stoichiometry of the TAA and Se powder. The elemental composition of the $ZnS_{1-x}Se_x$ nanosheets was measured by EDX and listed in Table 1. It can be seen the S/Se ratios of the resulting nanosheets are close to those of their corresponding precursors (TAA and Se powder) which indicates the relative reactivity between them was well balanced and the current synthetic strategy allowed for delicate control of the stoichiometry of $ZnS_{1-x}Se_x$ nanosheets. Besides, X-ray photoelectron spectroscopy (XPS) measurements of typical $ZnS_{0.4}Se_{0.6}$ nanosheets (Figure S7) were carried out to

investigate the surface composition, it was found that the surface S : Se ratio approaches to 0.37:0.63, which is consistent with the results of XRD and EDX.

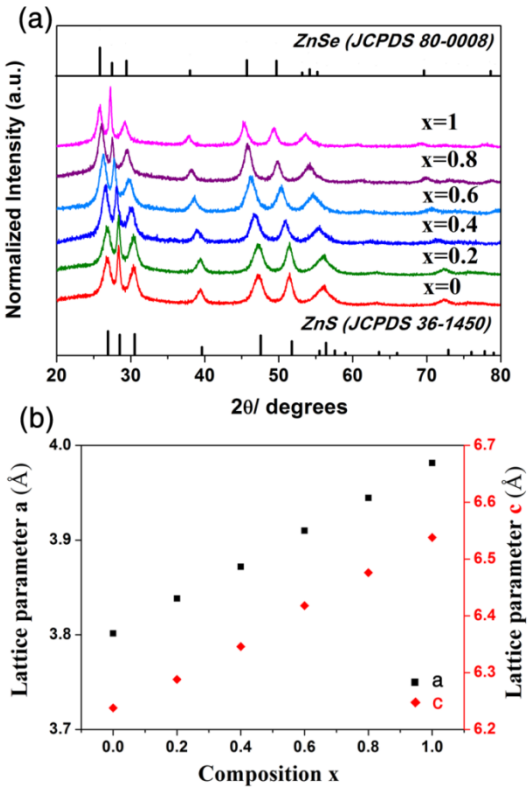

Figure 3 (a) XRD patterns of the $ZnS_{1-x}Se_x$ nanosheets for various values of x. The standard XRD patterns for ZnS and ZnSe were also shown as references. (b) A plot of the lattice constant "*a*" and "*c*" for various values of x.

Figure 3a shows the powder X-ray diffraction (XRD) patterns, which reveal that all the $ZnS_{1-x}Se_x$ nanosheets with various Se/S ratios have the similar diffraction pattern to those of hexagonal wurtzite phase ZnS and ZnSe (JCPDS: 36-1450 and 80-0008). Importantly, no secondary phase was detected in all diffraction patterns. Thus all $ZnS_{1-x}Se_x$ alloy nanocrystals are pure hexagonal wurtzite phase, which is consistent with the result of SAED in Figure 1d. We also observed the XRD peaks successively shift to lower 2θ degrees as the Se content increased, suggesting the lattice constants of $ZnS_{1-x}Se_x$ nanosheets become larger when the S atoms were gradually replaced by the larger Se atoms.[27, 28] The lattice parameters of $ZnS_{1-x}Se_x$ NCs were then determined from XRD data and the relationship between the lattice parameter and the chemical composition of $ZnS_{1-x}Se_x$ nanosheets was displayed in Figure 3b. We discovered a linear dependence of the lattice parameters on the composition, which is in accordance with Vegard's law.[32-34] This linear trend not only indicates a homogeneous element distribution of $ZnS_{1-x}Se_x$ nanosheets which is consistent with the results of EDS mapping in Figure 1c, but again corroborates that the chemical reactivity between TAA and Se powder was indeed well balanced.

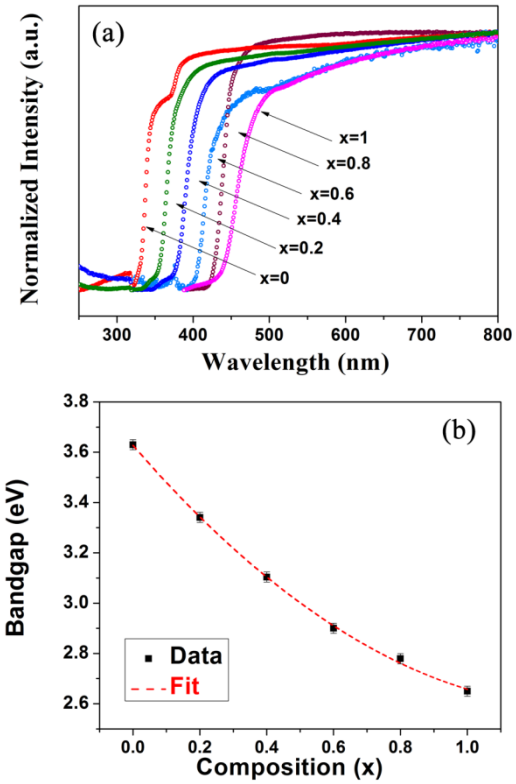

Figure 4 (a) The Normalized UV-vis diffuse reflectance spectra [a] of the $ZnS_{1-x}Se_x$ nanosheets with various Se content (x). (b) The dependence of bandgaps on the compositions of ternary $ZnS_{1-x}Se_x$ nanosheets.

[a] The effct of sintering temperature on the optical properties can be found in ESI.

The ability to control the chemical compositions and lattice parameters of $ZnS_{1-x}Se_x$ nanosheets would further allow us to tune their bandgaps and optical properties. Figure 4a shows the normalized UV-vis diffuse reflectance spectra of the $ZnS_{1-x}Se_x$ nanosheets with a series of Se/S ratios. The optic adsorption edge shows a systematic red-shift as the Se content increases from 0 to 1. Since hexagonal $ZnS_{1-x}Se_x$ is direct semiconductor,[34] we have applied Kubelka-Munk functions to the diffuse reflectance spectra to estimate the direct $([F(R)h\nu]^2)$ bandgaps.[35-37] The dependence of bandgaps on the chemical compositions is given in Figure 4b. The dash line is the fitted values from the bandgap relation of alloy nanosheets:

$$E_g^{ZnS_{1-x}Se_x} = x\,E_g^{ZnSe} + (1-x)\,E_g^{ZnS} - x\,(1-x)\,b$$

Where E_g^{ZnS} is bandgap of ZnS, E_g^{ZnSe} is bandgap of ZnSe, and b is the optical bowing parameter. The least-square fit yields b ca. 0.55 eV, which is consistent with previous experimental and theoretical reports.[27, 28, 34] Together, these tunable optical properties not only indicate the complete composition tunability of $ZnS_{1-x}Se_x$ nanosheets, but also demonstrate tunable bandgaps (2.62 - 3.66 eV) could be obtained.

In summary, we have successfully synthesized homogeneous non-layered $ZnS_{1-x}Se_x$ alloy nanosheets via thermal decomposition of lamellar inorganic-organic hybrid

precursors. The complete composition of alloy nanosheets could be easily obtained by changing the mole ratio of S / Se in the precursors. The lattice constants of $ZnS_{1-x}Se_x$ nanosheets have a linear dependence relationship on the Se content, and follow Vegard's law. The bandgaps of $ZnS_{1-x}Se_x$ nanosheets could be tuned from 2.62 to 3.66 eV via altering Se/S ratio in the nanoalloy. Our work provides a facile and effective strategy to synthesize homogeneous multinary chalcogenide nanosheets with a non-layered structure and manipulate their bandgaps and optical properties by tuning their chemical compositions.

Acknowledgments

We gratefully acknowledge the financial support by the NSF of China (91222204, 91122015, 21303202), 973 program (2013CB933200), and the NSF of Fujian Province (2012J05032).

Notes and references

1 J. H. Han, S. Lee and J. Cheon, *Chem. Soc. Rev.*, 2013, **42**, 2581.
2 M. Zhou, X. W. Lou and Y. Xie, *Nano Today*, 2013, **8**, 598.
3 C. N. R. Rao, H. S. S. Ramakrishna Matte and U. Maitra, *Angew. Chem. Int. Ed.*, 2013, **52**, 13162.
4 X. Huang, Z. Y. Zeng and H. Zhang, *Chem. Soc. Rev.*, 2013, **42**, 1934.
5 M. Chhowalla, H. S. Shin, G. Eda, L. J. Li, K. P. Loh and H. Zhang, *Nat. Chem.*, 2013, **5**, 263.
6 Y. F. Chen, J. Y. Xi, D. O. Dumcenco, Z. Liu, K. Suenaga, D. Wang, Z. G. Shuai, Y. S. Huang and L. M. Xie, *Acs Nano*, 2013, **7**, 4610.
7 Y. J. Gong, Z. Liu, A. R. Lupini, G. Shi, J. H. Lin, S. Najmaei, Z. Lin, A. L. Elias, A. Berkdemir, G. You, H. Terrones, M. Terrones, R. Vajtai, S. T. Pantelides, S. J. Pennycook, J. Lou, W. Zhou and P. M. Ajayan, *Nano Lett.*, 2014, **14**, 442.
8 H. Li, X. Duan, X. Wu, X. Zhuang, H. Zhou, Q. Zhang, X. Zhu, W. Hu, P. Ren, P. Guo, L. Ma, X. Fan, X. Wang, J. Xu, A. Pan and X. Duan, *J. Am. Chem. Soc.*, 2014, **136**, 3756.
9 H. M. Xu, G. Chen, R. C. Jin, D. H. Chen, J. Pei and Y. Wang, *CrystEngComm*, 2013, **15**, 5626.
10 J. J. Buckley, F. A. Rabuffetti, H. L. Hinton and R. L. Brutchey, *Chem. Mater.*, 2012, **24**, 3514.
11 Y. F. Sun, Z. H. Sun, S. Gao, H. Cheng, Q. H. Liu, J. Y. Piao, T. Yao, C. Z. Wu, S. L. Hu, S. Q. Wei and Y. Xie, *Nat. Commun.*, 2012, **3**.
12 Y. Sun, S. Gao and Y. Xie, *Chem. Soc. Rev.*, 2014, **43**, 530.
13 J. Joo, J. S. Son, S. G. Kwon, J. H. Yu and T. Hyeon, *J. Am. Chem. Soc.*, 2006, **128**, 5632.
14 S. Ithurria and B. Dubertret, *J. Am. Chem. Soc.*, 2008, **130**, 16504.
15 Y. H. Liu, V. L. Wayman, P. C. Gibbons, R. A. Loomis and W. E. Buhro, *Nano Lett.*, 2010, **10**, 352.
16 S. Ithurria, M. D. Tessier, B. Mahler, R. P. S. M. Lobo, B. Dubertret and A. Efros, *Nat. Mater.*, 2011, **10**, 936.
17 Z. Li and X. G. Peng, *J. Am. Chem. Soc.*, 2011, **133**, 6578.
18 J. Akhtar, M. Afzaal, M. Banski, A. Podhorodecki, M. Syperek, J. Misiewicz, U. Bangert, S. J. O. Hardman, D. M. Graham, W. R. Flavell, D. J. Binks, S. Gardonio and P. O'Brien, *J. Am. Chem. Soc.*, 2011, **133**, 5602.
19 Z. W. Quan, Z. P. Luo, W. S. Loc, J. Zhang, Y. X. Wang, K. K. Yang, N. Porter, J. Lin, H. Wang and J. Y. Fang, *J. Am. Chem. Soc.*, 2011, **133**, 17590.
20 J. J. Wang, D. J. Xue, Y. G. Guo, J. S. Hu and L. J. Wan, *J. Am. Chem. Soc.*, 2011, **133**, 18558.
21 X. Y. Huang, J. Li, Y. Zhang and A. Mascarenhas, *J. Am. Chem. Soc.*, 2003, **125**, 7049.
22 S. H. Yu and M. Yoshimura, *Adv. Mater.*, 2002, **14**, 296.
23 Z. X. Deng, C. Wang, X. M. Sun and Y. D. Li, *Inorg. Chem.*, 2002, **41**, 869.
24 Y. Xu, W. W. Zhao, R. Xu, Y. M. Shi and B. Zhang, *Chem. Commun.*, 2013, **49**, 9803.
25 J. Zhang, J. G. Yu, Y. M. Zhang, Q. Li and J. R. Gong, *Nano Lett.*, 2011, **11**, 4774.
26 L. Nasi, D. Calestani, T. Besagni, P. Ferro, F. Fabbri, F. Licci and R. Mosca, *J. Phys. Chem. C*, 2012, **116**, 6960.
27 M. Wang, G. T. Fei, Y. G. Zhang, M. G. Kong and L. De Zhang, *Adv. Mater.*, 2007, **19**, 4491.
28 H. Y. Xu, Y. Liang, Z. A. Liu, X. T. Zhang and S. K. Hark, *Adv. Mater.*, 2008, **20**, 3294.
29 J. D. Jiang, Q. Liao, Y. S. Zhao and J. N. Yao, *J. Mater. Chem.*, 2011, **21**, 4837.
30 J. Lu, H. Liu, C. Sun, M. Zheng, M. Nripan, G. S. Chen, G. M. Subodh, X. Zhang and C. H. Sow, *Nanoscale*, 2012, **4**, 976.
31 X. Ouyang, T. Y. Tsai, D. H. Chen, Q. J. Huang, W. H. Cheng and A. Clearfield, *Chem. Commun.*, 2003, 886.
32 K. Yu, A. Hrdina, J. Ouyang, D. Kingston, X. Wu, D. M. Leek, X. Liu and C. Li, *ACS Appl. Mater. Interfaces*, 2012, **4**, 4302.
33 L. Vegard, *Zeitschrift Fur Physik*, 1921, **5**, 17.
34 J. E. Bernard and A. Zunger, *Phys. Rev. B*, 1987, **36**, 3199.
35 Vanvecht.Ja and Bergstre.Tk, *Phys. Rev. B*, 1970, **1**, 3351.
36 S.-P. Guo, G.-C. Guo, M.-S. Wang, J.-P. Zou, H.-Y. Zeng, L.-Z. Cai and J.-S. Huang, *Chem. Commun.*, 2009, **29,** 4366.
37 M.-J. Zhang, X.-M. Jiang, L.-J. Zhou and G.-C. Guo, *J. Mater.Chem. C*, 2013, **1**, 4754.

Table of Contents

Facile Synthesis of Ternary Homogeneous $ZnS_{1-x}Se_x$ Nanosheets with Tunable Bandgaps

Jing Sun, Yumin Chen, Zhong-Ning Xu, Qing-Song Chen, Guan-E Wang, Ming-Jian Zhang, Gang Lu, Ke-Chen Wu* and Guo-Cong Guo*

State Key Laboratory of Structural Chemistry, Fujian Institute of Research on the Structure of Matter, Chinese Academy of Sciences, Fuzhou, Fujian 350002, P. R. China

Homogeneous ternary $ZnS_{1-x}Se_x$ nanosheets were easily fabricated through thermal decomposition of lamellar inorganic-organic hybrid precursors, and their complete composition and bandgap tunability were demonstrated.